35th Annual International Conference of the IEEE EMBS
Osaka, Japan, 3 - 7 July, 2013

Automatic correction of rotating Ultrasound Bio Microscopy acquisitions for the segmentation of the eye anterior segment*

C. Maindron, M. Le Loir, B. Cochener, M. Lamard

Abstract— **We have developed a rotating 3D probe prototype in order to acquire the anterior segment of the eye in three dimensions. The acquisition accuracy has to be sufficient to allow for the use of automatic segmentation of the provided data, and thus generate a 3D structure of the eye, for which it could be easier to obtain measurements than in 2D images.**

We have created an image post processing scheme in order to compensate for vibrations and eye movements during acquisition that are associated with increased noise.

These tools have been applied to 92 volume datasets acquired on 21 patients in pre-operative conditions. Acquisition noise was reduced by 97% in specific conditions with respect to data acquired without correction.

I. INTRODUCTION

Implantation of lenses within the eye is the standard of care for correction of visual defects such as myopia and hypermetropia. However its limited use is due to the lack of exact knowledge of the future positioning of the implant in the area between the iris and crystalline lens, the sulcus(fig. 1.a), of which three dimensions (3D) shape and dimensions are unknown[1][2][3]. Most ophthalmic devices are unable to see through the opacity of the iris. Therefore ultrasound technology was selected. Unfortunately, a standard ultrasound probe only takes a single acquisition of the eye, resulting in a 2D image.

In order to better understand the sulcus' structure we have developed a probe[4] that allows for 3D acquisitions of the posterior chamber in the anterior segment of the eye. This acquisition only lasts for a few seconds (~7-8 s.), however this duration is sufficient to render the acquisition sensitive to micro movements of the eye and/or the physician's hand, which leads to noisy 3D data reconstruction.

* This research is funded by Quantel Medical, Clermont-Ferrand, F-63808 France.

C. Maindron is with Université de Brest, INSERM, UMR 1101 LaTIM, SFR ScInBioS, 2 av Foch, Bat 1, Brest, F-29200 FRANCE, and with Quantel Medical, Clermont-Ferrand, F-63808 FRANCE (e-mail: charly.maindron@etudiant.univ-brest.fr).

M. Le Loir, is with CHRU Brest, Ophthalmological service, 2 av Foch, Bat 4, Brest, F-29200 FRANCE and with Université de Brest, INSERM, UMR 1101 LaTIM, SFR ScInBioS, 5 av Foch, Bat 1, Brest, F-29200 FRANCE (e-mail: matthieuleloir@gmail.com).

B. Cochener is with CHRU Brest, Ophthalmological service, 2 av Foch, Bat 4, Brest, F-29200 FRANCE and with Université de Brest, INSERM, UMR 1101 LaTIM, SFR ScInBioS, 5 av Foch, Bat 1, Brest, F-29200 FRANCE (e-mail: beatrice.cochener@ophtalmologie-chu29.fr).

M. Lamard is with Université de Brest, INSERM, UMR 1101 LaTIM, SFR ScInBioS, 2 av Foch, Bat 1, Brest, F-29200 FRANCE.
(e-mail: Mathieu.lamard@univ-brest.fr)

Acquisitions are carried out using a rotating ultrasound probe providing ultrasound images of the entire eye (fig. 1.a). These images have to be segmented in order to reconstruct the 3D volume. The goal of this work was to post process the acquired data to improve the automatic segmentation by correcting for acquisition errors thanks to specific image registering algorithms.

II. MATERIAL AND METHODS

A. Acquisitions

The rotating probe prototype used for the 3D acquisitions of the eye has been developed in collaboration by the Laboratory of Medical Information Processing (LaTIM INSERM UMR 1101) and Quantel Médical®. It consists of a combination of a conventional US probe Aviso® (Quantel Médical) containing a high frequency 50 MHz linear scanning transducer, with a step-by-step motor guidance AM1020-V-12-VM® (ARSAPE) (500 steps / second).

This innovative system allows for the acquisition of 30 coaxial slices along 180° (fig. 1.b), which has been assessed as the best compromise between accuracy and acquisition overall duration. Image size is 2048×1651 pixels (19.84×16mm).

Two mechanical motors are used in this probe. The first one allows for high speed linear translations of the piezoelectric element. The second one is placed outside the probe itself and allows for its rotation. These two combined movements lead to millimetric vibrations. Several acquisition setups were tested[5][6], including free hand (the user holds the probe), semi-rigid arm (the user is helped by a semi-rigid arm) and rigid arm (illustrated in fig. 2a, the user only guides the probe which is fixed on the rigid arm). We finally chose to equip the probe with the latter allowing for vertical movements, to assist the physician during the acquisition by reducing the vibrations associated with the rotation of the probe.

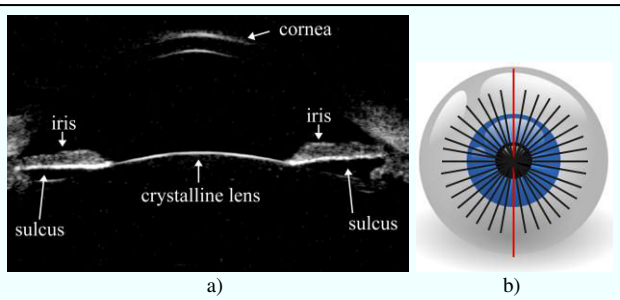

a) b)

Figure 1. a) Part of an US image of our acquisition. Anterior chamber of a human eye
b) Coaxial slice representation

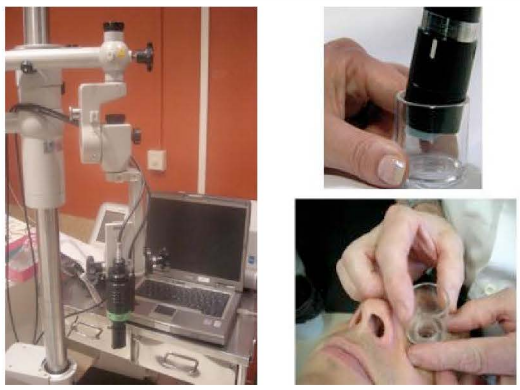

a) b)

Figure 2. a) Ultrasound probe on its arm
b) Eyecup® (top) and its positionning during acquisition (bottom)

B. Methods

- Data acquisition

Ultrasound acquisition requires the probe to be submerged in liquid, which is why an Eyecup® (Quantel Médical) (fig. 2b - top) with sterile water inside is placed on the eye. The physician has to keep the Eyecup® steady with one hand by applying sufficient pressure so the water does not leave the Eyecup®, while keeping the patient comfortable. Similar to the eye's movements, this leads to additional vibrations associated with increased noise in the acquired data (fig. 2b - bottom). Using his other hand, he will then guide the probe in the Eyecup® and let the rigid arm maintain the probe in position.

- Rotation axis calculation

Because our probe is a prototype, we do not have the direct knowledge of the rotation axis position. This rotation axis is in addition not perfectly aligned with the main axis of the probe (z axis). This information is however required for an accurate registration of the images in the volume and a 3D reconstruction of the eye. We first assumed the axis is placed along the z axis in the center of all the acquired images. However the first registration results clearly demonstrated this assumption did not hold (fig. 3). We therefore developed methods to estimate this axis with higher accuracy.

To validate the axis estimation we have used a phantom with known dimensions. This phantom is a methyl polymethacrylate cone frustum, with superior and inferior circles of 5 and 12 mm diameter respectively, and a 3mm height. We carried out acquisitions of this phantom and then each image was segmented and then reconstructed using different axes. The dimensions of each reconstructed object were compared with the real known dimensions of the phantom.

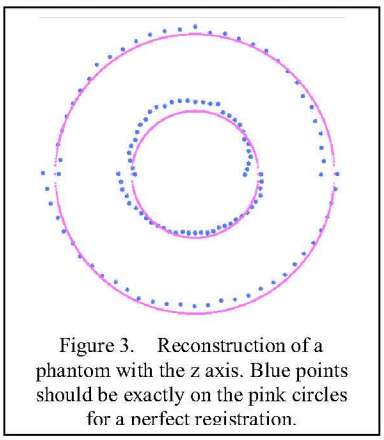

Figure 3. Reconstruction of a phantom with the z axis. Blue points should be exactly on the pink circles for a perfect registration.

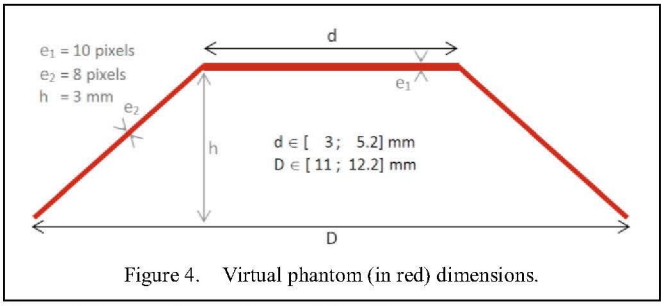

Figure 4. Virtual phantom (in red) dimensions.

We have developed an automatic accurate and reproducible segmentation algorithm consisting of generating a virtual phantom (only the external superior contour) defined by 5 parameters, as illustrated in fig 4: d, D, h, e1 and e2. h, e1 and e2 are fixed and not estimated during axis calculation.

The virtual phantom position is then optimized by maximizing a given criterion. Segmentation algorithm steps:

1. The pixel with highest intensity within the central pixel column of the image is automatically detected and selected. It will serve as a basis (x_0 ; y_0) for the positioning of the virtual phantom. In every acquisition we have made, this pixel belongs in all cases to the top part of the cone frustum.

2. Step 1 is repeated in another pixel column at a 1mm (104 pixels) distance from the central one, providing a new basis for the calculation of the phantom angle θ_0.

3. The research space for x, y (mm) and θ (°) is then defined as function of (x_0 ; y_0) and θ_0, and two parameters are used to modify the phantom dimensions: d and D (h, e1 and e2 are fixed) (mm). x, y and θ can take their values in [x_0-5 ; x_0+5], [y_0-5 ; y_0+5] and [θ_0-15 ; θ_0+15] respectively.

4. The entire parameter space is then explored. For each position of the virtual phantom, all pixels below it are summed and this value is considered as a figure of merit: the highest this sum, the closest the phantom is with respect to real position.

7. The virtual phantom position and angle associated with the highest figure of merit is selected and transferred to the next image, because this process is computationally expensive due to the large research space. It is therefore only calculated for the first image.

Indeed, we assume the movements between two consecutive slices are negligible and that the images are closely similar, allowing for the research space to be constrained.

On the next image i, the virtual phantom position in image i-1 is transferred and is used as the new initialization. The research space is constrained by defining the ranges at +/-0.5mm vertical and horizontal displacement and +/-3° rotation angle. The rest of the calculation is then very fast (see results).

For axis calculation, only the 4 extreme points of the virtual phantom (see fig. 5) on each image are used to characterize the structure and calculate the probe rotation axis.

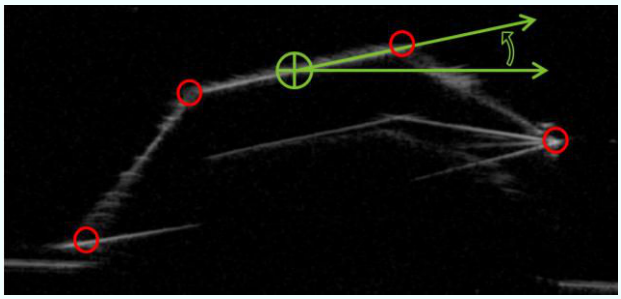

Figure 5. 4 extreme points in red and basis and angle in green.

In order to calculate this axis, the four points selected in each image are rotated around the same axis, to reconstruct the structure and quantify the error with respect to the real phantom. This is repeated as long as the figure of merit is insufficient.

1. The research space is defined along 4 dimensions (x , y , t_x , t_y): the four points rotate around an axis defined by a normalized vector V {obtained from vector V'(x ; y ; 1) with x , y ∈ [-0.2 ; 0.2] (mm)} which is displaced according to the translation vector T (t_x ; t_y ; 0) { t_x , t_y ∈ [-2.5 ; 2.5] (mm)} with steps of 0.01mm.

For the following points 2-4 the procedure is described for the superior side, however the inferior side is also processed.

2. For each new axis, the plane closest to the point cloud is determined through least squares estimation. The distance between the plane and the point cloud quantifies a first approximation error regarding the plane determination.

3. The point cloud is projected to the plane, which allows considering the problem in 2D instead of 3D.

4. The circle closest to the projected points is determined through least squares estimation. The distance between the circle and the projected point cloud quantifies a second approximation error regarding the circle determination.

5. We chose as the figure of merit the addition of the two approximation errors and the difference between circle diameters, as well as the height difference.

6. The axis minimizing this figure of merit is selected as the best axis.

This procedure was repeated for other acquisitions of the same phantom in different positions and we compared the best axes obtained. These should theoretically be the same and represent the rotation axis of the probe.

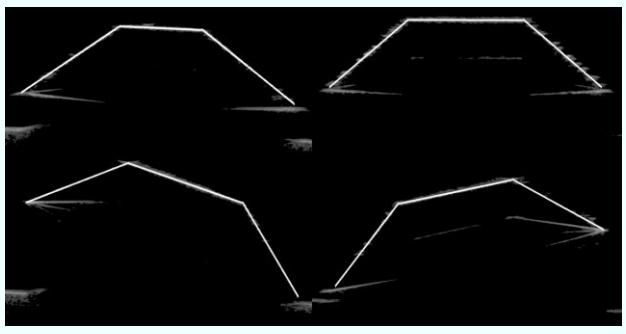

Figure 6. Examples of automatic segmentation results.

Once the axis has been obtained, it can be used to improve the reconstruction by applying it on the real acquisitions.

- Data vertical adjustment

This section is dedicated to correct for movements by the physician using post processing. Many registration methods have been proposed for use in the field of medical imaging[7][8][9]. However our application is very specific so we have developed a dedicated robust although simple algorithm to solve this issue. Lateral movements are impossible to detect in the images but we can correct vertical movements. The centers of each image in the volume are very close to each other, because of their proximity to the compared rotation axis. This is why we chose to compare vertically variations of the central pixel column of each image in order to detect vertical movements.

1. The algorithm is first initialized by selecting as a reference the central column of image 0.

2. On each image i, the central column of pixels is compared to the one from image 0.

3. The sum of absolute differences between grey levels pixel-to-pixel is calculated and used as a figure of merit.

4. Step 3 is repeated to calculate the differences between pixel *j* in image 0 and pixel *j+k* in image i for k ∈ [-100 ; 100].

5. The optimal vertical displacement of image I is the one k minimizing the figure of merit.

Obtained displacements are then applied to each image in order to obtain a vertical adjustment of the acquisitions for a better registration.

C. Patients

21 patients were included with 40 acquired eyes, leading to 92 data volumes. 13 myopic patients (24 eyes) and 8 hypermetropic patients (16 eyes) underwent an implantation by one surgeon using Anterior Chamber Intra Ocular Lens Acrisof ® Cachet™ (Alcon) [10] and Posterior Chamber Intra Ocular Lens V4 (STAAR Surgical®)[11].

III. Results

A. Data acquisitions

TABLE I. EFFICIENCY OF THE PROBE: ACQUISITION DURATION

Number of slices	***30***	***60***	***100***
Duration (sec)	7.4	10.3	17.5

TABLE II. QUANTIFIED ERRORS DUE TO MOVEMENT DEPENDING ON THE PROBE ASSIST SYSTEM.

Assist system	***None (free hand)***	***Semi-rigid arm***	***Rigid arm***
Mean movement (mm)	3.2 +/- 0.8	1.4 +/- 0.4	0.1* +/- 0.1

* Errors associated with movement were reduced by 97% and 93% with respect to free hand and semi-rigid arm respectively

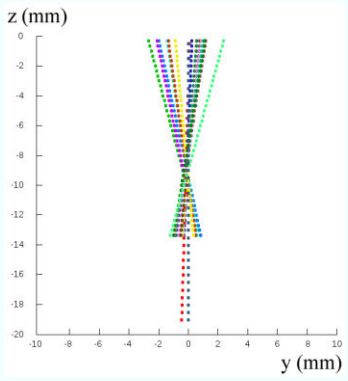

Figure 7. All estimated axes. Variations along the x axis are negligeable.

B. *Rotation axis*

The automatic segmentation method is more accurate (fig. 6) and faster. For 100 images, the entire process takes 3min and 34 sec (33 sec for the first image and 1.8 sec for each other image) with an HP Z-400 4 cores 2.67GHz 8G RAM vs. 1hour and 30min for manual segmentation. 18 Different positions of the phantom were segmented.

The calculation of the rotation axis has been carried out on all these 18 different volumes, leading to different although very close results (fig. 7). We have demonstrated that the rotation axis was different in each acquisition and that it is therefore impossible to determine without mechanical intervention on the motor and the probe. However, all estimated axes are very close to the z axis and the mean error with respect to real axis was 0.02 mm (+/- 0.015mm) when choosing the vertical axis. Therefore this was the one used for all other reconstructions.

C. *Vertical adjustment*

The vertical adjustment was instantaneous and a synthetic image is generated before and after registration to provide a visual check of the registration quality (fig. 8). A mean 0.12mm (11 pixels) (+/-0.28mm) vertical fitting was observed over 92 acquisitions. Registration results were visually assessed by experts to be accurate and better adjusted to the fitted data.

We applied this improvement within the context of automatic segmentation relying on the deformation of a 3D model of the eye to the patient data and found that it led to an 8% Hausdorff distance decrease vs. the use of raw data.

IV. Conclusion

This work demonstrated that the probe rotation axis was always different in each acquisition but that assuming this axis was the z axis led to low error in subsequent reconstructions.

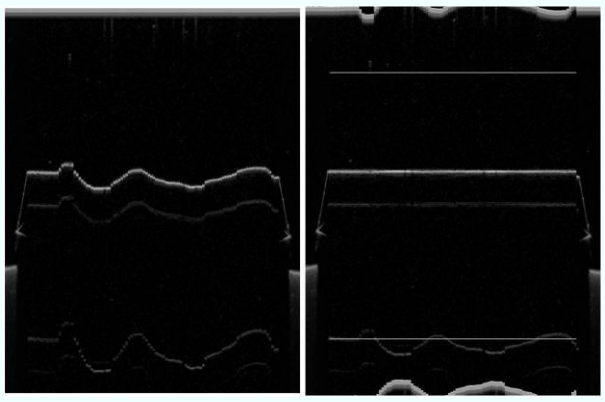

Figure 8. Synthetic images. Before (on the left) and after (on the right) vertical adjustment

We also developed a vertical adjustment method relying on vertical registration that allowed for a significant improvement over raw data for the reconstruction. This improved reconstruction provides some interesting perspectives especially regarding the automatic model-based segmentation of the eye that we are currently developing.

Future work will consist in improving the research space exploration using for instance genetic algorithms, in order to optimize computational cost.

We will continue developing automatic segmentation of the eye in order to build a software granting the physician a real time access to the 3D structure of the eye currently scanned.

As a final step, we will introduce within our model the laws describing mechanical properties of the eye structures [12] [13] in order to simulate the eye structural modifications introduced by the phakic IOL positioning [14].

Acknowledgment

We acknowledge Mathieu Hatt for his help.

References

[1] Kawamorita T et al. ” Relationship between ciliary sulcus diameter and anterior chamber diameter and corneal diameter”, *J Cataract Refract Surg. 2010 Apr*

[2] Petermeier K et al. “Sulcus anatomy and diameter in pseudophakic eyes and correlation with biometric data: evaluation with a 50 MHz ultrasound biomicroscope.” *J Cataract Refract Surg. 2012 Jun*

[3] Kim KH et al. “Correlation between ciliary sulcus diameter measured by 35 MHz ultrasound biomicroscopy and other ocular measurements.” *J Cataract Refract Surg. 2008 Apr*

[4] Le Loir M et al.” Application de la reconstruction en trois dimensions du segment antérieur par échographie haute fréquence à l’implantation phaque de chambre postérieure ”. *Phd Thesis, Université de Bretagne Occidentale, Faculté de Médecine*. 2011.

[5] Josselin PM et al. ” Reconstruction en 3D du segment antérieur par échographie haute fréquence ; application au dimensionnement des implants phaques. ” *Phd Thesis* 2009

[6] Cochener B et al. ” 3 Dimensional Free-Hand Reconstruction of Ocular Anterior Segment Using Hight Frequency Ultra-Sounds ”. *Brest : s.n.*, 2010.

[7] Liren Zhu et al. “A robust registration method for real-time ultrasound image fusion with pre-acquired 3D dataset” *Engineering in Medicine and Biology Society,EMBC, 2011 Annual International Conference of the IEEE*

[8] Pagoulatos, N. et al. “Fast calibration for 3D ultrasound imaging and multimodality image registration”, *BMES/EMBS Conference, 1999. Proceedings of the First Joint*

[9] Francois, R. et al. “Robust statistical registration of 3D ultrasound images using texture information”, *Image Processing, 2003. ICIP 2003. Proceedings. 2003 International Conference on*

[10] Mastropasqua L et al. ” AcrySof cachet phakic intraocular lens in myopic patients: visual performance, wavefront error, and lens position” , *J Refract Surg. 2012 Apr*

[11] Le Loir M et al. ” Long-term results of posterior chamber phakic intraocular lens implantation for correction of high ametropia” , *J Fr Ophtalmol. 2012 Jun*

[12] Ciarlet, P.G. ” Elasticité tridimensionnelle” , *Paris : Masson*, 1985. 2-225-80724-8.

[13] Jouve, F. ” Modélisation de l’œil en élasticité non-linéaire” , *Phd Thesis, Université Paris VI*. 1992.

[14] Hecht, ” F. FreeFem++” , *Third Edition, Version 3.12. Laboratoire Jacques-Louis Lions, Université Pierre et Marie Curie, Paris : s.n.*, 2010.